Precision of predicted 3D numerical solutions of vortex-induced oscillation for bridge girders with span-wise varying geometry

Takehiko Harada[†], Takeshi Yoshimura[‡], Takahisa Tanaka[†],
Yoji Mizuta[‡] and Takafumi Hashiguchi[†]

Department of Civil Eng., Kyushu Sangyo University, Higashi-Ku, Fukuoka, 813-8503, Japan

Makoto Sudo[‡†]

Ingérosec Co., Ltd., 6-3-1 Nishishinjuku, Shinjuku-Ku, Tokyo, 160-0023, Japan

Masao Miyazaki[‡‡]

Sumitomo Heavy Industries, Ltd., Shinagawa-Ku, Tokyo, 141-8686, Japan

Abstract. A method of numerical analysis without conducting 3D wind tunnel model tests was examined in our previous study for predicting vortex-induced oscillation of bridge girders with span-wise varying geometry. The aerodynamic damping forces measured for plural wind tunnel 2D models were used in the analysis. A further study was conducted to examine the precision of solution obtained by this method. First, the responses of vortex-induced oscillation of two rocking models and a taut-strip bridge girder model with span-wise varying geometry were measured. Next, the responses of these models were numerically analyzed by means of this method, and then a comparison was made between the obtained Vr-A-δ_a contour diagram of each 3D model in the wind tunnel test and the diagram in the numerical analysis. Since close correlations were observed between each two Vr-A-δ_a diagrams obtained in the model test and in the analysis in cases where the 3D model did not have strong three-dimensionality, our findings revealed that the predicted solution proved to be reasonably accurate.

1. Introduction

In our previous paper (Yoshimura, *et al.* 2001), the amplitude of vortex-induced oscillation was predicted for a medium-span sine-curved hybrid cable-stayed bridge with span-wise varying

---

† Graduate Student
‡ Professor
‡† Vice-President
‡‡ General Manager

geometry. 3D wind tunnel model studies are generally conducted in order to examine the aerodynamic behavior of such bridges as they have a 3D geometrical shape. However, the wind tunnel available for our study had a working section of only a 1.5 m square cross-section, which was not sufficiently wide to conduct 3D model tests. Therefore, it was necessary to develop the following alternative method for predicting the amplitude of oscillation of the full-scale bridge: first, the aerodynamic damping forces were measured for plural 2D models in the wind tunnel; next, a linearized method for a 3D numerical analysis was prepared, and then applied to predict the amplitude of oscillation for this bridge.

Another reason why 2D models were used was that our study was conducted at its preliminary design stage when the cheaper 2D model tests were preferable to the more expensive 3D model tests. However, once the precision of the solution obtained by means of this alternative analytical method is proved to be sufficiently high to predict vortex-induced oscillation of full-scale bridges, this method can be applicable to their detailed wind resistant design by using a small-size wind tunnel. Based on this consideration, further studies were conducted to examine the precision of the predicted solution. The results of these findings were partially reported at AWAS'02 Conference (Harada, *et al*. 2002), but complete details of these results are reported in this paper.

2. Abstract of previous study

An abstract of our previous study (Yoshimura, *et al*. 2001) on vortex-induced oscillation of the hybrid cable-stayed bridge shown in Fig. 1 is described in this section. The transverse inclination and the width of the girder respectively vary from -9 to +9 % and from 23.7 to 25.6 m along the bridge axis as its horizontal alignment has a sine curve with a maximum radius of curvature of 280 m.

First, the aerodynamic damping forces were measured for seven kinds of 1:40 scale 2D models denoted by <1> to <7> in Fig. 1(b) where the arrow denotes the wind direction. Fig. 2 shows the amplitude dependent aerodynamic damping coefficients, $H_1^*(z)$, obtained at one of the wind speeds tested. $H_1^*(z)$ between <1> and <2>, ..., and <6> and <7> were obtained by linear interpolation. Next, the lowest natural mode and frequency in vertical bending shown in Fig. 3(b) were obtained by the eigenvalue analysis using the finite element analytical model shown in Fig. 3(a). The aerodynamic damping forces were input to the nodal points of the analytical model, and the time-
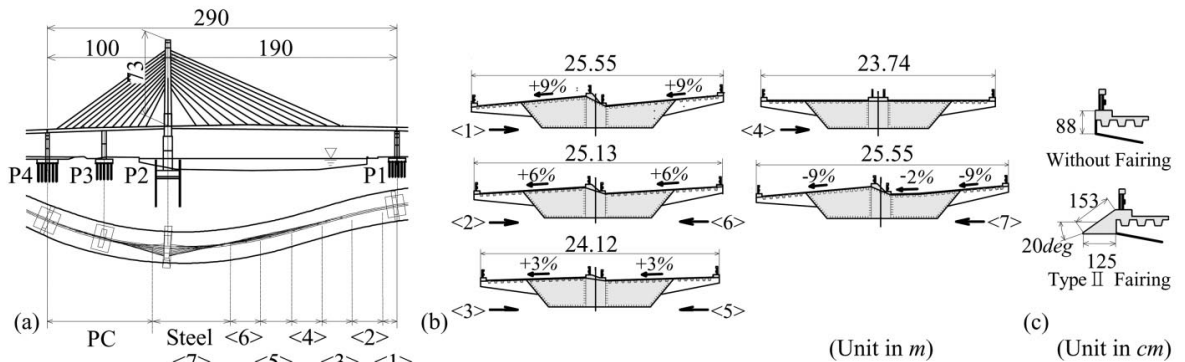

Fig. 1 Sine-curved hybrid cable-stayed bridge. Elevation and plane figure (a); cross-sections of girder with transverse inclinations of +9, +6, ... -6 and -9% (b); and one of triangular fairings examined (c)
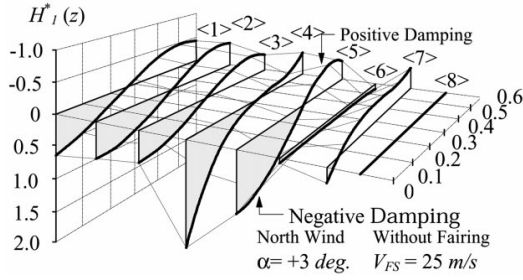
Fig. 2 Amplitude dependent aerodynamic damping coefficients of girder, $H_1^*(z)$, with seven transverse inclinations obtained in wind tunnel 2D model tests
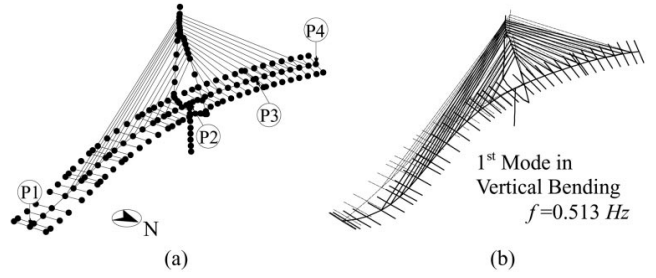
Fig. 3 Finite element model used in 3D numerical analysis (a); and natural mode and frequency in 1st mode in vertical bending (b)
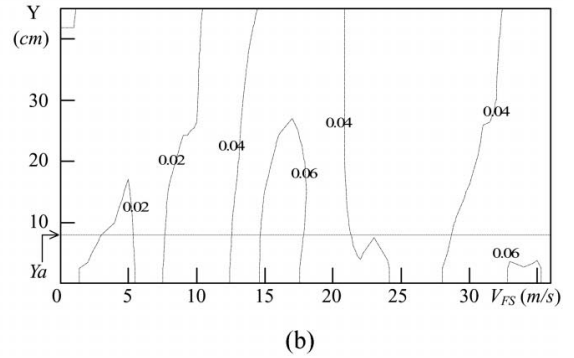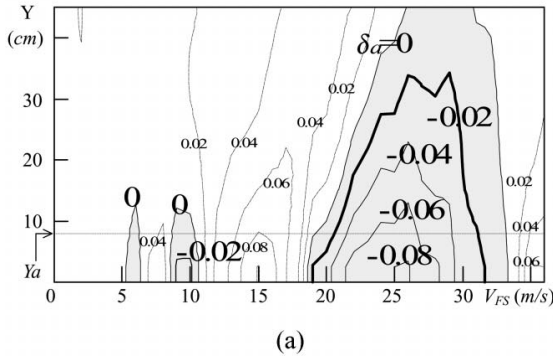

Fig. 4 V-A-δ_a contour diagrams for girders without and with one of triangular fairings examined, (a) and (b), obtained in 3D numerical analysis

history response at this wind speed was analyzed. From the results analyzed in the rage of wind speed of 5 to 40 m/s, so-called V-A-δ_a contour diagrams shown in Figs. 4(a) and (b) were obtained (δ_a: the aerodynamic damping in logarithm; Figs. (a) and (b): the results for the girder with and without one of the triangular fairings shown in Fig. 1(c)). The findings in these figures revealed that the triangular fairings examined was able to suppress the excitation perfectly for the deck with the structural damping of 0.02 in logarithm as can be seen in Fig. 4. Based on these findings, it was decided that the bridge girder with this fairing had to be included in the detailed design.

The findings in a further study revealed that the solutions with high precision could be obtained by using not seven but only three combinations of $H_1^*(z)$ for three 2D models.

3. Examination process

A better way of examining the precision of the predicted solutions is to make a comparison between the response of the cable-stayed bridge in Fig. 1 in the 3D wind tunnel model test and the response in the numerical analysis. However, the cross-section of wind tunnel working section is not sufficiently wide to conduct 3D model tests of this bridge as described above. Therefore, the examination was conducted by using different 3D wind tunnel models from this cable-stayed bridge
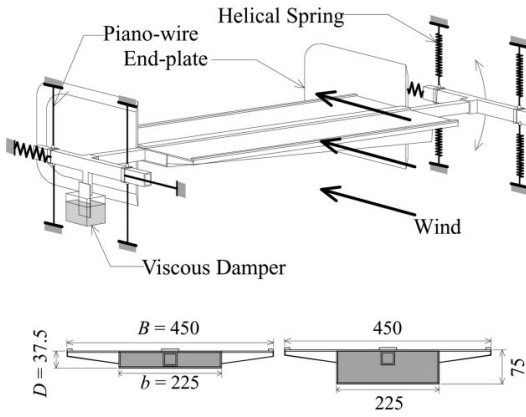
Fig. 5 Rocking bridge girder wind tunnel model with span-wise varying 'depth'
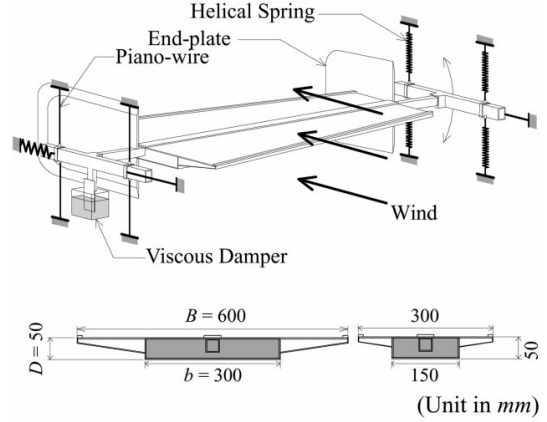
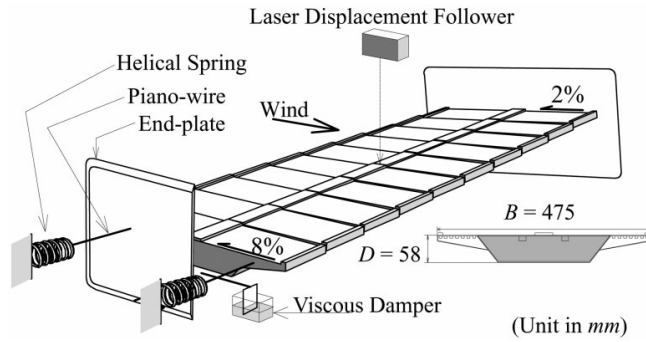Fig. 6 Rocking bridge girder wind tunnel model with span-wise varying 'width'

Fig. 7 Taut-strip bridge girder wind tunnel model with varying transverse inclination

model.

In general, bridge girders with span-wise varying geometry are characterized by varying their transverse inclination, depth and/or width. In this study, three kinds of 3D wind tunnel models were prepared for the examination: a rocking model whose 'depth' varied along the model axis maintaining both the transverse inclination and width constant (Fig. 5); another rocking model whose 'width' varied maintaining the other two constant (Fig. 6); and a taut-strip model whose 'transverse inclination' varied maintaining the other two constant (Fig. 7). First, the response of vortex-induced oscillation was measured for each 3D model in the wind tunnel by the free vibration method and Vr-A-δ_a contour diagram was obtained. Next, the response of each 3D model was numerically analyzed by means of the modal analysis used in our previous study (Yoshimura, *et al.* 2001). The non-linear aerodynamic damping coefficients, $H_1^*(z)$, measured for plural wind tunnel 2D models (so called Vr-A-$H_1^*(z)$ contour diagrams: reduced wind speed - amplitude - $H_1^*(z)$ diagrams) were used in the analysis. Then, a comparison was made between Vr-A-δ_a contour diagram of each 3D model in the wind tunnel test and the diagram in the numerical analysis.

4. Details of wind tunnel models

4.1. Rocking models

One of the rocking bridge girder models shown in Fig. 5 had a constant deck width (B) of 450 mm with span-wise varying depth (D) from 37.5 to 75 mm: the side ratio of cross-section (D/B) varied from 1/12 to 1/6. While, another rocking model shown in Fig. 6 had a constant depth of 50 mm with span-wise varying width from 600 to 300 mm: D/B also varied from 1/12 to 1/6. The bottom plate width of these models (b) was half the deck width. In order to induce the rocking motion in vertical bending, one of the model ends was suspended by helical springs, while the motion of another model end was restrained by piano-wires. A viscous damper was installed for vibration control in span-wise direction. The natural mode and frequency of one of the models (Fig. 5) is shown in Fig. 8.

4.2. Taut-strip model

As shown in Fig. 7, the 475 mm wide, 58 mm deep and 140 mm long ten bridge girder model segments were suspended by a pair of highly pre-stressed piano-wires. Each piano-wire was connected to a hard helical spring on its end, and viscous dampers were installed for vibration control in windward direction. Although these segments had the same cross-section, their transverse inclinations (the angle of attack), i, varied along the model axis from +2 to +8 deg. (from +3.5 to 14 %) in a windward direction as shown in Figs. 7 and 9(b). This taut-strip model had one of the 1/50 scale cross-sections of the cable-stayed bridge girder denoted by <4> in Fig. 1(b). For the sake of simplicity, this model had no handrails, and the mass and the structural damping were not simulated (the model had much smaller Scruton number than the required value). The 2 mm gap between two adjoining segments was sealed with a 0.1 mm thick silicon elastic film. The lowest natural mode and frequency in vertical bending are also shown in Fig. 9.
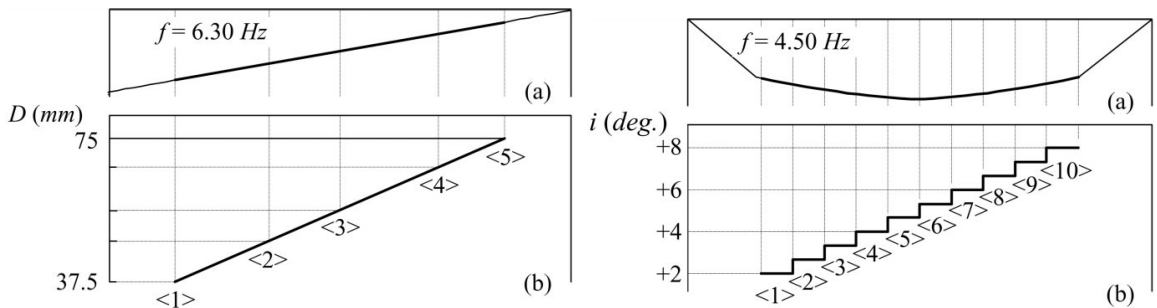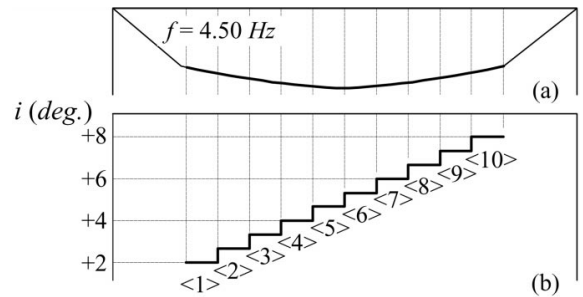

Fig. 8 Natural mode of rocking model (a) with span-wise varying depth (b)

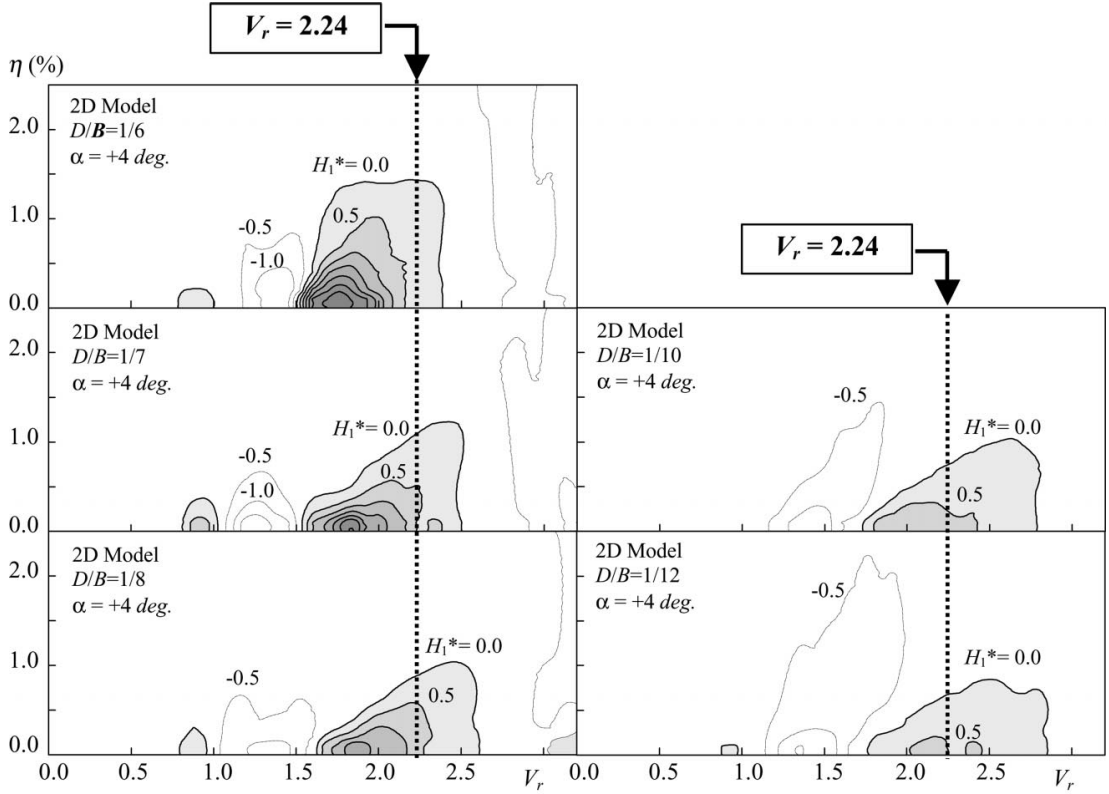Fig. 9 Natural mode of taut-strip model (a) with span-wise varying transverse inclination (b)

Fig. 10 Vr-A-$H_1^*(z)$ contour diagrams of five 2D models with different side ratios
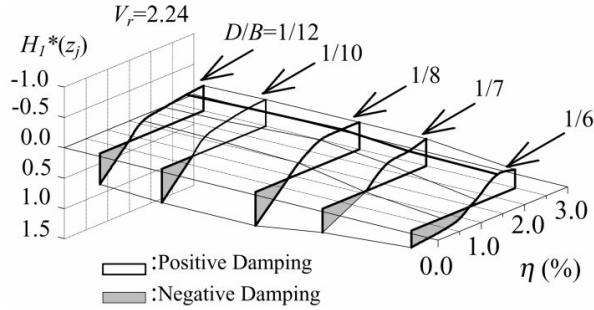

Fig. 11 $H_1^*(z)$ curves based on strip theory, so interpolated that they have to be denoted by lines between measured five $H_1^*(z)$ curves

5. Vr-A-$H_1^*(z)$ contour diagrams for numerical analyses

5.1. Rocking models

Since the side ratio of cross-section (D/B) for two rocking models varied along the model axis from 1/12 to 1/6 as described above, five 2D models with D/B=1/12, 1/10, 1/8, 1/7 and 1/6 were made to obtain five Vr-A-$H_1^*(z)$ contour diagrams which were used in the numerical analyses. The
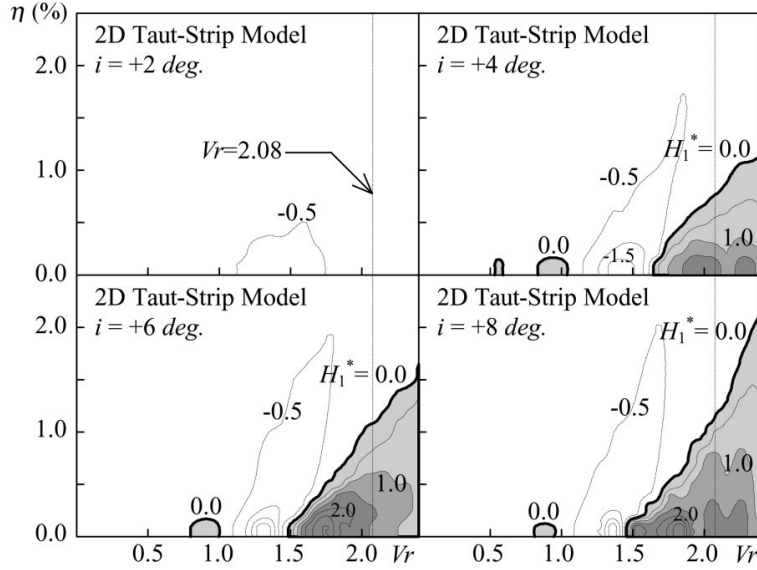
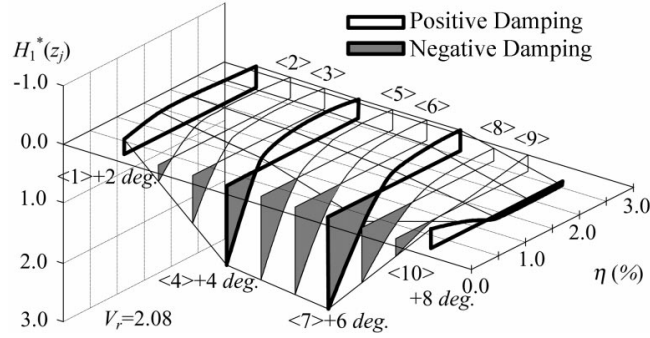Fig. 12 *Vr-A-$H_1^*(z)$* contour diagrams of four 2D models with different transverse inclinations

Fig. 13 Six $H_1^*(z)$ curves obtained by linear interpolation together with four $H_1^*(z)$ curves measured at *Vr*=2.08

deck width (*B*) of these models has a constant value of 450 mm and the deck depth (*D*) varied 37.5, 45, ... and 75 mm. The non-dimensional aerodynamic damping coefficient $H_1^*(z)$ was obtained by means of the free vibration method and was defined by $H_1^*(z)=-\mu\delta_a/\pi$, where $\mu= m/(\rho_a\lambda^2)$ is the reduced mass, *m* the mass per unit length, ρ_a the air density, and $\lambda=B$ for 3D model with constant *B* (Fig. 5) or $\lambda=D$ for the one with constant *D* (Fig. 6).

Fig. 10 shows *Vr-A-$H_1^*(z)$* contour diagrams obtained for these five 2D models. In the figure, the ordinate and the abscissa respectively represent the non-dimensional amplitude of displacement, $\eta= y/B$, and the reduced wind speed, $Vr=V/(fB)$, where *y* is the amplitude of displacement, *V* the wind speed and *f* the frequency. *Vr-A-$H_1^*(z)$* contour diagrams for 2D deck models with *D/B* between 1/12 and 1/10, ..., and 1/7 and 1/6 were obtained by linear interpolation. For example, $H_1^*(z)$ curves at the reduced wind speed of 2.24 were so interpolated that they had to be denoted by the lines between the measured five $H_1^*(z)$ curves shown in Fig. 11.

5.2. Taut-strip model

Since the transverse inclination (wind angle of attack) of the ten segments in the taut-strip model varied along the model axis from +2 to +8 deg. as described above, ten Vr-A-$H_1^*(z)$ contour diagrams were necessary for the numerical analysis. Ten segments of the taut-strip model were connected tightly to each other to form a '2D taut-strip model' with transverse inclination of 0 deg. The wind angles of attack of the 2D taut-strip model tested were +2, +4, +6 and +8 deg. that corresponded to the transverse inclinations of the segments <1>, <4>, <7> and <10> in Fig. 9.

Fig. 12 shows Vr-A-$H_1^*(z)$ contour diagrams for the segments <1>, <4>, <7> and <10>. Vr-A-$H_1^*(z)$ contour diagrams for other six segments were obtained by linear interpolation. For example, the interpolated six $H_1^*(z)$ curves together with the measured four $H_1^*(z)$ curves at the reduced wind speed of 2.08 are shown in Fig. 13.

6. Outline of method for 3D numerical analyses

The rocking model used in the numerical analysis is shown in Fig. 14(a). The model span was divided into forty elements with equal length of Δs_j. The nodal point 'j' was located at each element center and the equivalent lumped mass, m, was connected at the spring-mounted model end. In the figure, $z_j(t)$ is the displacement of the nodal point 'j' at time 't' and $L_j(t)$ the aerodynamic damping force acting on the element. While, each segment of the taut-strip model was divided into three elements and a lumped mass m_j of the element was located at its nodal point (Fig. 14(b)).

Consider the analytical taut-strip or rocking model oscillating in wind. Although $L_j(t)$ is non-linear, dependent on the amplitude z_j of the displacement $z_j(t)$, an approximate solution can be obtained under the following conditions: in each half of the cycle, only the fundamental harmonic component of the aerodynamic damping force with the amplitude proportional to $H_1^*(z_j)$ $\dot{z}_j$ is taken into account ($\dot{z}_j$: the amplitude of velocity at the nodal point j). Under this piece-wise linearized condition, the modal analysis can be applied by using the finite element analytical model (Fig. 14),
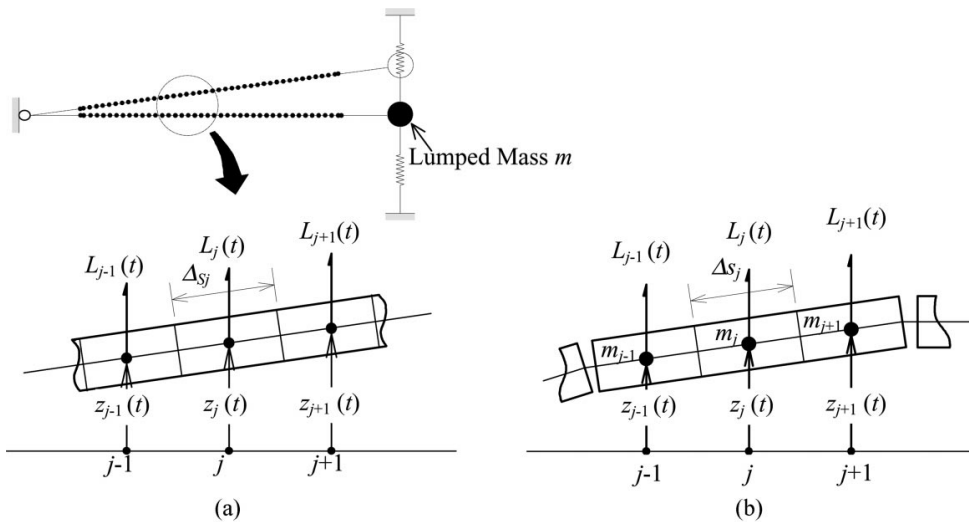

Fig. 14 Rocking model (a) and taut-strip-model (b) used in numerical analysis

and according to Scanlan (1978) and Simiu and Scanlan (1978), the aerodynamic damping force input to the nodal point 'j' is expressed by

$$L_j(t) = (\rho_a \cdot B_j^2 \cdot \omega \cdot H_1^*(z_j) \cdot \Delta s_j) \cdot \dot{z}_j(t) \tag{1}$$

In this study, only vortex-induced oscillation in vertical bending in 1st mode was examined, that is, other higher modes in vertical bending and torsional modes were not considered. Therefore, the superposition of modes was not necessary, and the equation of motion and the displacement vector $\{z(t)\}$ are respectively expressed by Eqs. (2) and (3).

$$\ddot{q}(t) + 2h_s \cdot \omega \cdot \dot{q}(t) + \omega^2 \cdot q(t) = \frac{L(t)}{M} \tag{2}$$

$$\{z(t)\} = [\{\varphi\}_1, ..., \{\varphi\}_K, ..., \{\varphi\}_N] \cdot (0, ..., 0, q_K(t), 0, ..., 0)^T = \{\varphi\}_K \cdot q_K(t) \equiv \{\varphi\} \cdot q(t) \tag{3}$$

In the above equations, $q(t)$ represents the modal coordinate; $h_s = \delta_s/(2\pi)$ the modal damping ratio obtained in the experiment (depending on the amplitude of displacement); ω the natural circular frequency (experimental value in Figs. 8 and 9); $M = \{\varphi\}^T \cdot [M] \cdot \{\varphi\}$ the modal mass; $[M]$ the mass matrix; $L(t) = \{\varphi\}^T \cdot \{L(t)\}$ the modal aerodynamic damping force; $\{L(t)\}$ the aerodynamic damping force vector with 'j' component, $L_j(t)$, given by Eq. (1); $[\varphi]$ the mode vector (experimental value, Figs. 8 and 9). All the components in $[M]$ are zero except (n, n) component of 'm' for the rocking model. Substitution of the velocity vector, $\{\dot{z}(t)\}$, expressed by Eq. (4) into $\{L(t)\}$ gives Eq. (5).

$$\{\dot{z}(t)\} = \{\varphi\} \cdot \dot{q}(t) \tag{4}$$

$$L(t) = \left[\rho_a \cdot \omega \sum_j B_j^2 \cdot H_1^*(z_j) \cdot \varphi_j^2 \cdot \Delta s_j\right] \cdot \dot{q}(t) \tag{5}$$

Thus, the term on the right in Eq. (2) is rewritten as

$$L(t)/M = \{\varphi\}^T \cdot \{L(t)\}/M = 2 \cdot h_a \cdot \omega \cdot \dot{q}(t) \tag{6}$$

where h_a is the modal 'aerodynamic' damping ratio and is expressed by Eq. (7).

$$h_a = \frac{\frac{1}{2} \cdot \rho_a \sum_j B_j^2 \cdot H_1^*(z_j) \cdot \varphi_j^2 \cdot \Delta s_j}{\sum_i \sum_j M_{ij} \cdot \varphi_i \cdot \varphi_j} = -\frac{\delta_a}{2\pi} \tag{7}$$

By using Eqs. (6) and (7), Eq. (2) is rewritten as

$$\ddot{q}(t) + 2 \cdot (h_s - h_a) \cdot \omega \cdot \dot{q}(t) + \omega^2 \cdot q(t) = 0 \tag{8}$$

There are two ways to obtain the solution at a given wind speed. One is the way where the 'non-linear' Eq. (8) with 'non-linear' aerodynamic damping ratio, h_a, is solved by means of the Newmark beta method and the time-history response, that is, the 'divergent', 'convergent' or 'steady-amplitude' oscillation can be obtained. Another is the way where δ_a at a given amplitude of $q(t)$ can directly be obtained by using Eq. (7) in only 'steady-amplitude' oscillation. It was verified that the solutions obtained by both ways could result in the same solution in 'steady-amplitude' oscillation.

7. Comparison of results in wind tunnel 3D model tests and those in numerical analyses

7.1. Rocking models

Vr-A-δ_a contour diagrams of the rocking models obtained in the wind tunnel 3D model tests and the diagrams in the numerical analyses are shown in Figs. 15-18 where Figs. (a) and (b) respectively illustrate the experimental and the analytical results. In these figures, the numbers on each contour represent the aerodynamic damping in logarithm (δ_a) and the shadowed area the negative damping region where the excitation was observed. Very close correlations can be observed between the experimental and the analytical results for the model with span-wise varying 'depth' in both cases where the model end with shallow deck was spring-mounted (or moving, Fig.
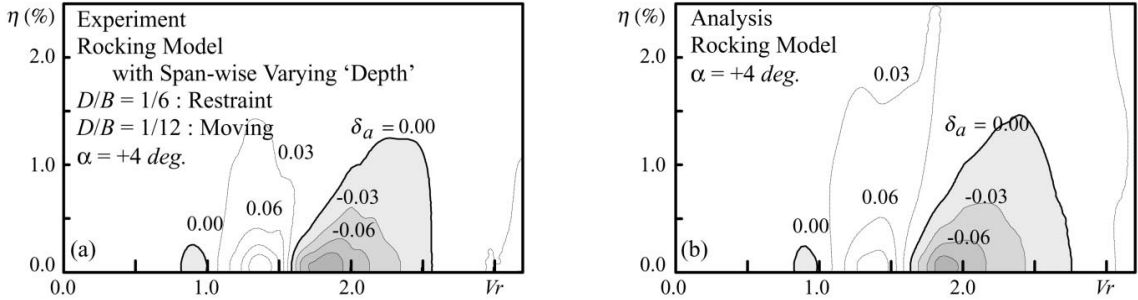

Fig. 15 Vr-A-δ_a contour diagrams of rocking model with span-wise varying 'depth' and with 'shallow deck moving' obtained in wind tunnel (a) and diagram in numerical analysis (b)
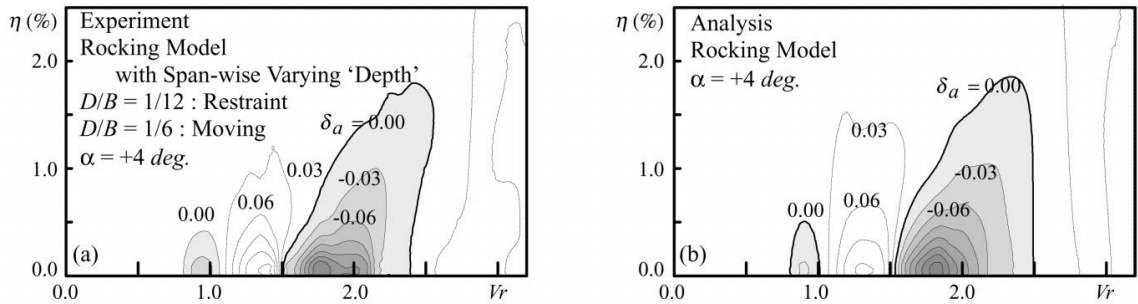

Fig. 16 Vr-A-δ_a contour diagrams of rocking model with span-wise varying 'depth' and with 'deep deck moving' obtained in wind tunnel (a) and diagram in numerical analysis (b)
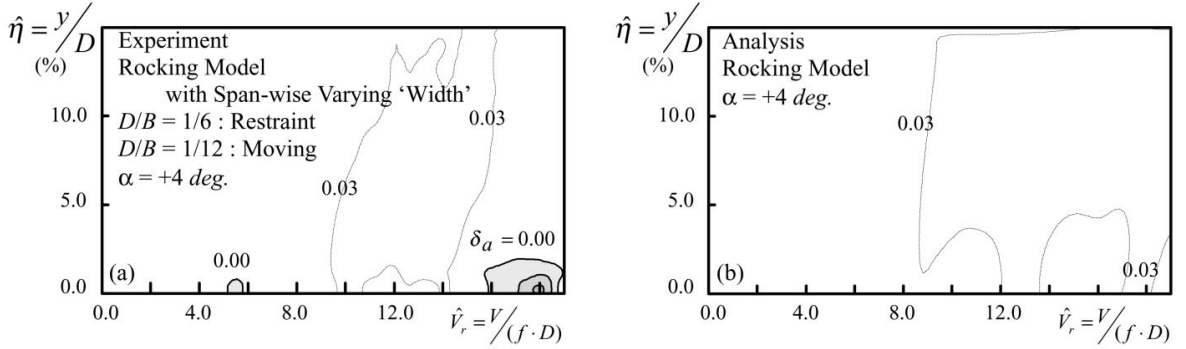
Fig. 17 Vr-A-δ_a contour diagrams of rocking model with span-wise varying 'width' and with 'shallow deck moving' obtained in wind tunnel (a) and diagram in numerical analysis (b)
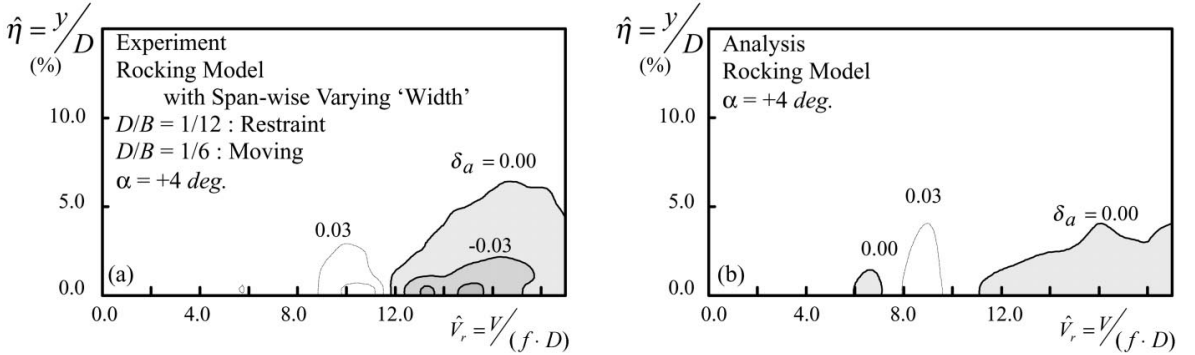

Fig. 18 16 Vr-A-δ_a contour diagrams of rocking model with span-wise varying 'width' and with 'deep deck moving' obtained in wind tunnel (a) and diagram in numerical analysis (b)

15) and the one with deep deck moving (Fig. 16). On the other hand, different response characteristics were observed between the experimental and the analytical results for the rocking model with span-wise varying 'width' (Figs. 17 and 18).

7.2. Taut-strip model

The experimental and the analytical results of the taut-strip model with span-wise varying transverse inclination from +2 to +8 deg. together with the ones with a constant value of +6 deg. are respectively illustrated in Figs. 19 and 20. The wind tunnel model responses in the range of reduced wind speed (Vr) above 2.6 are not shown in these figures as the transition of mode from vertical bending to torsion was observed at about Vr=2.7. Furthermore, it was difficult to obtain the free vibration records with sufficiently high precision in this wind speed range as plural unstable limit-cycles were observed. Fairly close correlations are observed in these figures between the experimental and the analytical results.

A supplementary examination was conducted for the 2D taut-strip model. In the numerical analysis, the mode vector $\{\varphi\}=\{1\}$ was substituted into Eq. (3). Much closer correlations can be observed between Figs. 21 (a) and (b).
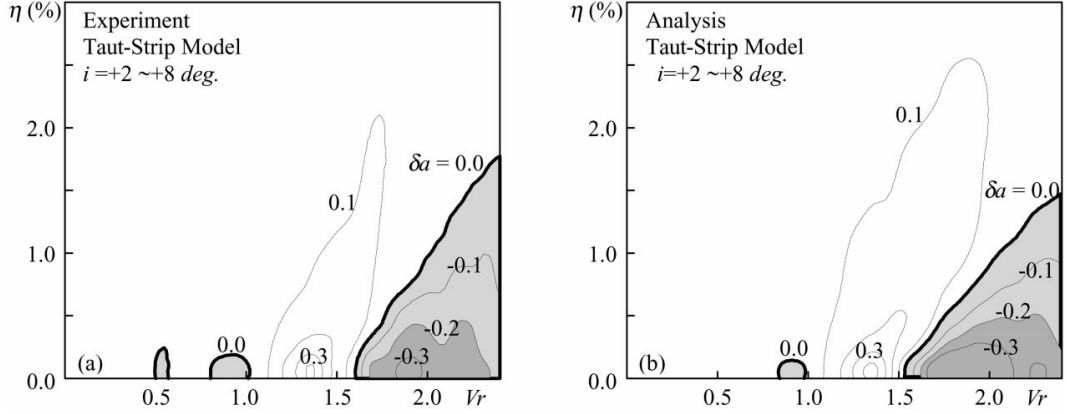
Fig. 19 Vr-A-δ_a contour diagram of taut-strip model with span-wise varying transverse inclination obtained in wind tunnel (a) and diagram in numerical analysis (b)
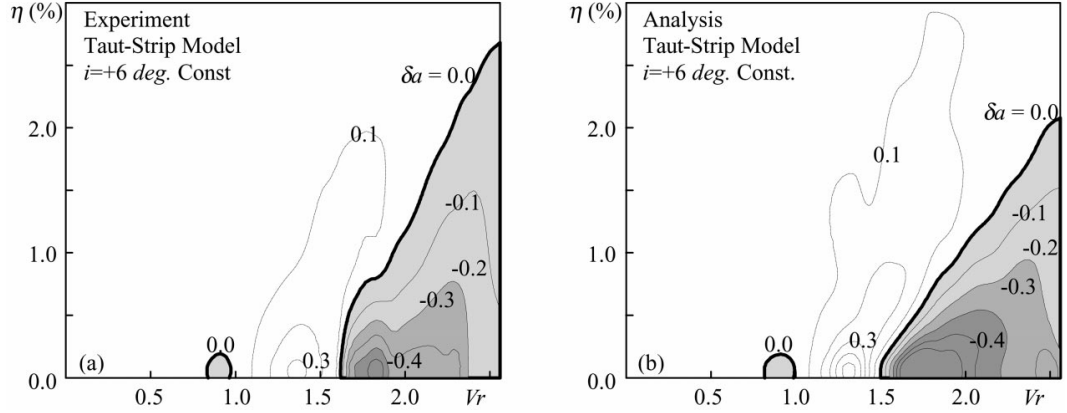

Fig. 20 Vr-A-δ_a contour diagram of taut-strip model with constant transverse inclination obtained in wind tunnel (a) and diagram in numerical analysis (b)
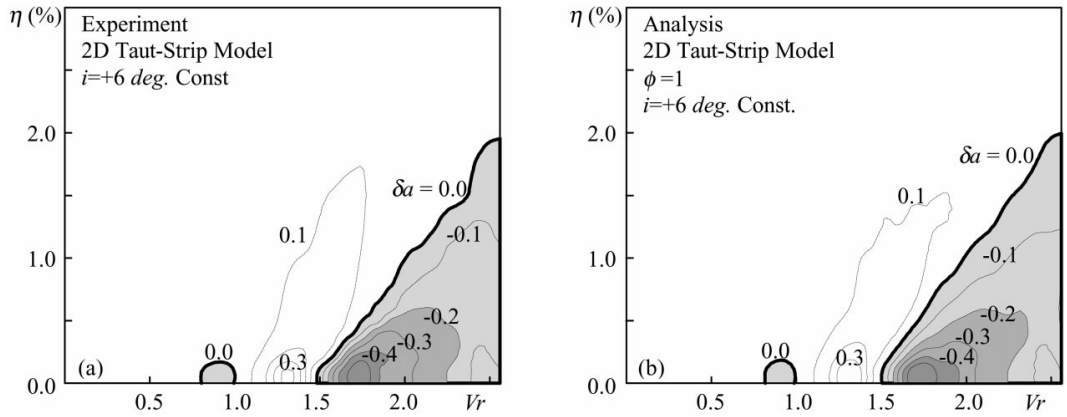

Fig. 21 Vr-A-δ_a contour diagram of 2D taut-strip model obtained in wind tunnel (a) and diagram in numerical analysis (b)

8. Precision of numerically predicted solutions and discussion

8.1. Precision of solutions

In the previous section, 'qualitative' comparisons were made between Vr-A-δ_a contour diagrams obtained in the wind tunnel tests and the diagrams in the numerical analyses. In order to discuss the precision of numerically predicted solutions shown in Figs. 15-21, 'quantitative' comparisons had to be made except Figs. 17 and 18 where different response characteristics were observed between the experimental and the analytical results. In this study, the error of solutions were estimated by the following procedures: first, the ratio of the analytical to the experimental values on the following three terms was estimated on each contour with the same value of δ_a: the 'maximum amplitude', the 'critical wind speed' where the excitation started (on-set) and the 'super-critical wind speed' where the excitation ended. Then, the mean value was calculated for each term. In the error estimation of the maximum amplitude, the weighted mean value was calculated. For example, the weight of 1/5 was taken into account in the case where the maximum amplitude on a contour was one-fifth of the absolute maximum amplitude.

The findings for the rocking model with span-wise varying depth and the taut-strip model are respectively summarized in Figs. 22 and 23 in terms of error (positive: over-estimated). In these figures, 'low-speed excitation' represents the small amplitude excitation observed in lower reduced wind speed range centered at around 0.9 and 'high-speed excitation' the large amplitude excitation in higher speed range centered at around 1.8.

Of all the cases, the error in the critical and the super-critical wind speeds denoted by a full triangle and an 'x', respectively was smaller than that in the maximum amplitude denoted by a full circle. As for the rocking model, the findings revealed that the maximum errors were about 5 and 10% in the cases of shallow deck moving ((a) in Fig. 22) and deep deck moving ((b) in Fig. 22),
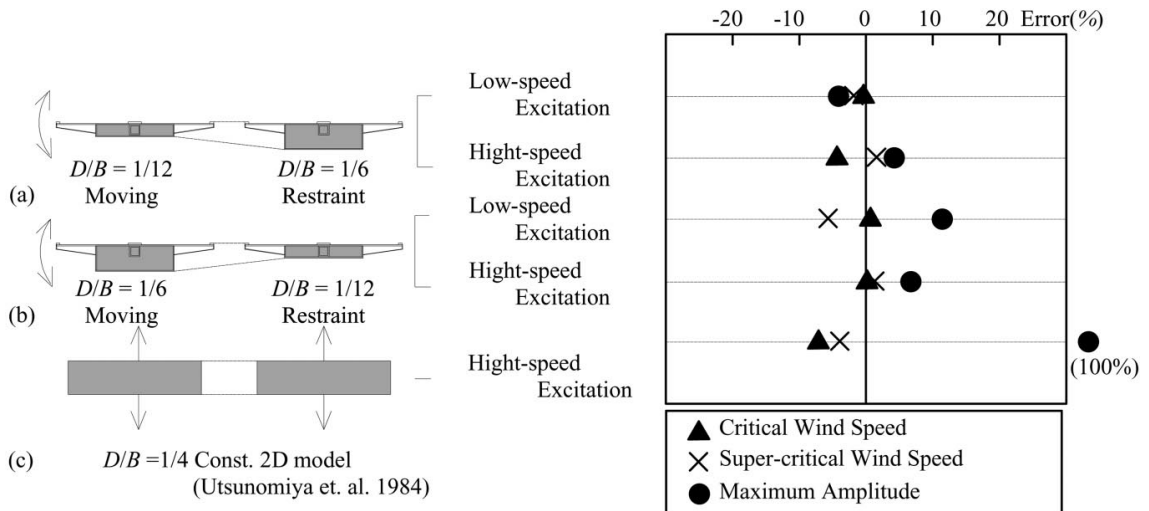
Fig. 22 Errors of predicted numerical solutions in maximum amplitude, critical wind speed and super-critical wind speed for rocking model with span-wise varying depth
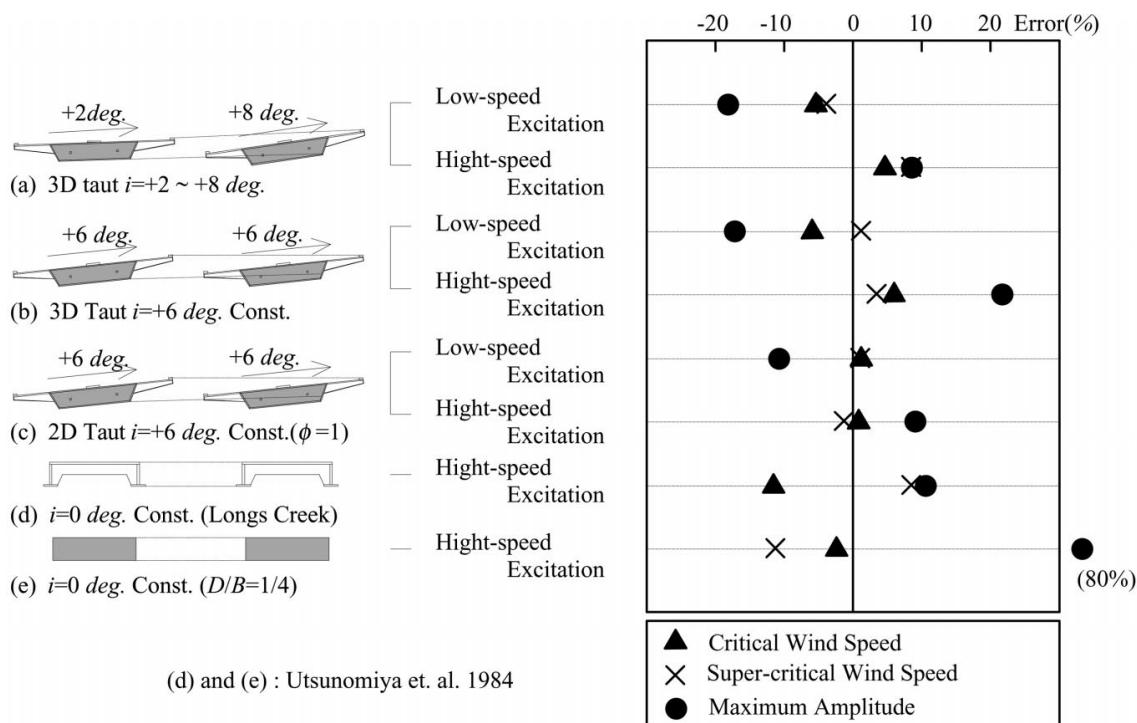
Fig. 23 Errors of predicted numerical solutions in maximum amplitude, critical wind speed and super-critical wind speed for taut-strip model

respectively. On the other hand, in the cases of the 3D and 2D taut-strip models, the maximum errors were about 20% and 10%, respectively ((a, b) and (c) in Fig. 23).

8.2. Discussion

8.2.1. Rocking models

The error of 10% for the rocking model with 'varying depth' and with 'deep deck moving' ((b) in Fig. 22) was twice the value for the one with 'shallow deck moving' ((a) in Fig. 22). The secondary flow formed on the model close to the end-plate is thought to be one of the possible causes of the larger error as the ratios of the end-plate height of 30 cm to the model depth of 7.5 and 3.8 cm for these two cases were 4 and 8, respectively: the former was not sufficiently large (end-plate size effects). One of the causes of the error of 100% in the 2D rectangular model shown in Fig. 22(c), which was reported by Utsunomiya (1984), was probably due to be the end-plate size effects.

As for the rocking model with varying 'width' (Figs. 17 and 18), the secondary flow due to strong three-dimensionality is thought to be one of the possible causes of the different response characteristics. The reason for this was that the taper angle of this model deck width was 12 deg.: considerably larger than that of the deck depth of 1.5 deg. for the model with varying 'depth'.

8.2.2. Taut-strip models

The error of 20% observed in the 3D taut-strip model ((a) and (b) in Fig. 23) is most likely due to the following causes: the end-plate size effects; the secondary flow due to 3D geometrical shape; the transition of mode which is characteristic of multi-degree-of-freedom systems; the existence of a few unstable limit-cycles[1]; and the technical problem to introduce very high tensile force in a pair of piano-wires. The error of 80% in the taut-strip model tests shown in Fig. 23(e), which was reported by Utsunomiya (1984), was probably due to the same causes.

8.2.3. Precision of solution presented in our previous study

In short, the solution obtained by means of the linearized method examined in our previous study (Yoshimura, *et al*. 2001) proved to be reasonably accurate in predicting the response of vortex-induced oscillation for bridge girders with span-wise varying geometry in cases where the girders did not have strong three-dimensionality and where the size of the end-plate of 2D models for measuring the aerodynamic damping force was sufficiently large compared to the model depth.

9. Conclusions

In order to examine the precision of solution, which was obtained by the linearized method provided in our previous study for predicting vortex-induced oscillation of bridge girders with span-wise varying geometry, the responses of vortex-induced oscillation of two rocking and a taut-strip bridge girder models were measured first in the wind tunnel. The depth, the width or the transverse inclination of each model varied along its axis maintaining the other two constant so as to form the 3D geometrical shapes. From these 3D model test results, Vr-A-δ_a contour diagram was obtained for each model. In the next stage, the response of each model was numerically analyzed by means of this method. Vr-A-$H_1^*(z)$ contour diagrams obtained in 2D wind tunnel model tests were used in the analyses. Then, comparisons were made between the obtained Vr-A-δ_a contour diagram of each 3D model in the wind tunnel test and the diagram in the numerical analysis. In order to estimate the precision of solutions quantitatively, the ratio of the analytical to the experimental values on the following three terms was calculated on each contour: the 'maximum amplitude', the 'critical wind speed' and the 'super-critical wind speed' where the excitation ended, and then the mean value of the ratios, that is, the error was calculated for each term.

Our findings revealed that the errors of 5-10% were observed in one of the rocking models and a 2D taut-strip model, and that the error of 20% was observed in the 3D taut-strip model. Also the error could hardly be estimated in another rocking model which had strong three-dimensionality as different response characteristics were observed between the experimental and analytical results. The axial secondary flow formed on the model due to 3D geometrical shape as well as insufficient size of the end-plate are thought to be one of the possible causes of the error above 10%. In the 3D taut-strip model, the error is most likely due to the following causes: the transition of mode which is characteristic of multi-degree-of-freedom systems; the existence of a few unstable limit-cycles; and

---

[1]An initial amplitude of velocity was imposed to the 2D model not by an actuator but by hands in the free vibration method. Since the model had a little high natural frequency of about 6 Hz, there was a difficulty in finding out the amplitude of a few unstable limit-cycles exactly.

the technical problem of introducing very high tensile force in a pair of piano-wires.

Findings of our study revealed that the solutions were reasonably accurate in predicting the response of vortex-induced oscillation for bridge girders with span-wise varying geometry in cases where the girders did not have strong three-dimensionality and where the size of the end-plate was sufficiently large compared to the model depth.

Acknowledgements

References

Harada, T., Yoshimura, T., Mizuta, Y., Tanaka, T., Hashiguchi, T., Noda, S. and Sudo, M. (2002), "A further study on prediction of vortex-induced oscillation of bridge girders with span-wise varying geometry", *Proc. 2nd International Symposium on Advances in Wind & Structures,* 307-314.

Scanlan, R.H. (1978), "The action of flexible bridges under wind: flutter theory", *J. Sound Vib*., **60**(2), 201-211.

Simiu, E. and Scanlan, R.H. (1978), *Wind Effects on Structures*, John-Wiley, 220-229.

Utsunomiya, H., Nagao, F. and Hatakeyama, K. (1984), "Some investigations on the wind tunnel test of the aerodynamic behaviors of bluff bodies", *Proc. 8th National Symposium on Wind Engineering,* 327-332.

Yoshimura, T., Mizuta, Y., Yamada, F., Umezaki, H., Shinohara, T., Machida, N., Tanaka, T. and Harada, T. (2001), "Prediction of vortex-induced oscillation of a bridge girder with span-wise varying geometry", *J. Wind Eng. Ind. Aerodyna.*, **89**, 1717-1728.

CC